Models and Numerical Methods for Environmental Problems. Part III: Fire Propagation Models

Luis Ferragut
Institute on Fundamental Physics and Mathematics and Department of Applied Mathematics, University of Salamanca, Spain

Abstract

The contain of this lecture is mainly taken from [1] and [2].

1 Nomenclature

Physical quantities

T	temperature
T_∞	reference temperature
T_f	flame temperature
E	enthalpy
D	density of the porous fuel bed
M	fuel load
D_s	gas density
K	thermal conductivity of the porous fuel bed
C	heat capacity
C_g	gas heat capacity
H	flame height
M_v	moisture content
Λ_v	evaporation latent heat
Λ_p	pyrolysis heat

2 Governing equations

The dimensionless equations governing the fire spread in a region Ω with boundary Γ are:

$$\partial_t e + \mathbf{w}.\boldsymbol{\nabla} e - \kappa \Delta u + \alpha u = R(u, y) \tag{2.1}$$

$$e \in G(u) \tag{2.2}$$

$$\partial_t y = -g(u) y\,. \tag{2.3}$$

The boundary and initial conditions are given, respectively, by

$$u(\mathbf{x}, t) = 0\,, \quad \mathbf{x} \in \Gamma,\ t > 0 \tag{2.4}$$

$$u(\mathbf{x}, 0) = u_0(\mathbf{x})\,, \quad \mathbf{x} \in \Omega \tag{2.5}$$

$$y(\mathbf{x}, 0) = y_0(\mathbf{x})\,, \quad \mathbf{x} \in \Omega\,. \tag{2.6}$$

The unknowns $e = \frac{E}{MCT_\infty}$, $u = \frac{T - T_\infty}{T_\infty}$ and y are the dimensionless enthalpy, the dimensionless temperature and the mass fraction of solid fuel, respectively. y_e is the mass fraction lower bound of extinction. $\mathbf{w} = \frac{D_g C_g}{DC}\mathbf{v}$ is a re-scaled velocity and g is defined by $g(u) = s^+(u, y)\beta$ where the function s^+ is given by

$$s^+(u, y) = \begin{cases} 1 & \text{if} \quad u \geq u_p \text{ or } y > y_e \\ 0 & \text{otherwise} \end{cases}$$

The non-dimensional enthalpy e is an element of a multivalued operator G, given by:

$$G(u) = \begin{cases} u & \text{if} \quad u < u_v \\ [u_v\ ,\ u_v + \lambda_v] & \text{if} \quad u = u_v \\ u + \lambda_v & \text{if} \quad u_v < u < u_p \\ [u_p + \lambda_v\ ,\ u_p + \lambda_v + \lambda_p] & \text{if} \quad u = u_p \\ u + \lambda_v + \lambda_p & \text{if} \quad u > u_p\,, \end{cases}$$

where u_v and u_p are the non-dimensional evaporation temperature of the water and the non-dimensional pyrolysis temperature of the solid fuel, respectively. The quantities λ_v and λ_p are the non-dimensional evaporation heat and pyrolysis heat, respectively and are related to the physical quantities by

$$\lambda_v = \frac{M_v \Lambda_v}{C T_\infty}$$

$$\lambda_p = \frac{\Lambda_p}{C T_\infty}\,.$$

The convective term $\mathbf{w}.\boldsymbol{\nabla} e$ takes into account the energy convected by the pyrolisated gas through the elementary control volume.
The right hand side describes the thermal radiation from the flame above the layer. A

derivation of this term is given in the appendix. This term is a convolution operator given by,

$$R(\mathbf{x}) = \delta \int_{\Omega_f(u,y)} f(\mathbf{x} - \tilde{\mathbf{x}})\, d\tilde{\mathbf{x}}$$

which takes into account nonlocal radiation from the flame, where $\delta = \frac{a\sigma T_f^4}{\pi DCT_\infty}[t][l]$, $[t]$,$[l]$ are the time scale and length scale respectively, and $\Omega_f(u,y) = \{x \in \Omega;\ u(x) > u_p \text{ and } y(x) > y_e\}$ is the fire domain on the surface.
The term $\kappa\Delta u$ describes thermal conduction and αu represents the energy lost by convection in the vertical direction. The parameters κ and α are related to physical quantities by $\kappa = \frac{k[t]}{DC[l]^2}$ and $\alpha = \frac{h[t]}{DC}$.
Equation (2.3) represents the fuel mass variation by pyrolysis.
It should be noticed that in the burnt zone the multivalued operator does not exactly represent the physical phenomena as the water vapor is no more in the porous medium. This drawback can be circumvented setting $\lambda_v = 0$ and $\lambda_p = 0$ in the burnt area.
These model is a variant of the models in [7] (chapter one), Model I in [6] or model in [8] where we have introduce the influence of the moisture content and the heat absorption by pyrolysis, by using the enthalpy multivalued operator. The nonlocal radiation term used in this paper is derived in the appendix.

3 Numerical method

3.1 *Time integration*

Let $\Delta t = t^{n+1} - t^n$ a time step and let y^n, e^n and u^n denote approximations at time step t^n, to the exact solution y, e and u respectively.
We consider a semi-implicit scheme by discretizing the total derivative, see [10]

$$\partial_t e + \mathbf{w}.\boldsymbol{\nabla} e \approx \frac{1}{\Delta t}(e^{n+1} - \bar{e}^n)$$

where $\bar{e}^n = e^n \circ \mathbf{X}^n$, and $\mathbf{X}^n(\mathbf{x}) = \mathbf{X}(\mathbf{x}, t^{n+1}, t^n) \approx \mathbf{x} - \mathbf{w}\Delta t$ is the position at time t^n of the particle which is at position $\mathbf{x}$ at time t^{n+1}. At each time step we solve,

$$\frac{y^{n+1} - y^n}{\Delta t} = -y^{n+1} g(u^{n+1}) \tag{3.1}$$

$$\frac{e^{n+1} - \bar{e}^n}{\Delta t} - \kappa\Delta u^{n+1} + \alpha u^{n+1} = R^n \tag{3.2}$$

$$e^{n+1} \in G(u^{n+1})\,. \tag{3.3}$$

The basic idea is to treat implicitly the positive terms. Instead the nonlocal radiation term, which is costly computed, is evaluated explicitly at time t^n.

3.2 *Iterative solution at each time step*

Problem (3.1),(3.2),(3.3) is non linear due to the multivalued operator G. We consider first an exact perturbation of this problem.
Let $\omega > 0$ be a given parameter and set

$$G^\omega = G - \omega I$$

where I is the identity; then (3.3) can be written

$$z^{n+1} = e^{n+1} - \omega u^{n+1} \in G^\omega(u^{n+1})\,. \tag{3.4}$$

For λ and ω verifying $\lambda\omega < 1$, the resolvent

$$J^\omega_\lambda = (I + \lambda G^\omega)^{-1} = ((1-\lambda\omega)I + \lambda G)^{-1}$$

is a well defined univalued operator and the Yosida approximation of G^ω is given by

$$G^\omega_\lambda = \frac{I - J^\omega_\lambda}{\lambda}\,.$$

It is easy to check that inclusion (3.4) is equivalent to equation

$$z^{n+1} = G^\omega_\lambda(u^{n+1} + \lambda z^{n+1})\,.$$

This suggests the following algorithm for solving (3.1), (3.2), (3.3):
For u^n, y^n and z^n, given

1. Set $u^{n+1,0} = u^n$, $z^{n+1,0} = z^n$.
2. Compute
$$y^{n+1,i+1} = \frac{y^n}{1 + \Delta t g(u^{n+1,i})}\,.$$
3. Compute $u^{n+1,i+1}$ solving
$$(\alpha\Delta t + \omega)u^{n+1,i+1} - \Delta t\kappa\Delta u^{n+1,i+1} = \bar{e}^n - z^{n+1,i} + \Delta t R^n\,.$$
4. Compute $z^{n+1,i+1} = G^\omega_\lambda(u^{n+1,i+1} + \lambda z^{n+1,i})\,.$
5. If $\|z^{n+1,i+1} - z^{n+1,i}\| > Tol$, update $i \leftarrow i+1$ and go to step 2,
else, end of the loop.

For $\lambda\omega \le 1/2$ the Yosida approximation G^ω_λ is Lipschitz operator with constant $1/\lambda$ and the convergence of the algorithm can be proved [11].

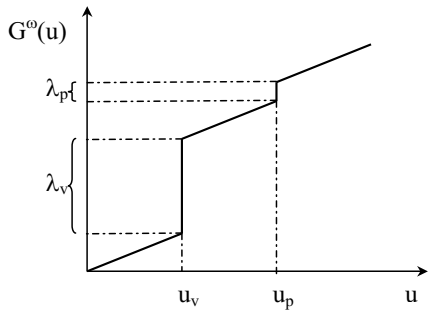

Figure 1: G^ω operator

3.3 *Practical computation of* $z^{n+1,i+1}$

In the following we take $\lambda\omega = 1/2$. Set $\bar{u} = u^{n+1,i+1} + \lambda z^{n+1,i}$, then

$$G^\omega_\lambda(\bar{u}) = \frac{1}{\lambda}\bar{u} - \frac{1}{\lambda}J^\omega_\lambda(\bar{u})\,.$$

It remains to explain how to calculate

$$\bar{z} = J^\omega_\lambda(\bar{u})\,,$$

which is equivalent to solve (for $\lambda\omega = \frac{1}{2}$)

$$(\omega I + G)\bar{z} \ni 2\omega\bar{u}\,.$$

Then s is given by (*Figure 1*):

if	$2\omega\bar{u} < (1+\omega)u_v$	then	$\bar{z} = \frac{2\omega\bar{u}}{1+\omega}$
if	$(1+\omega)u_v < 2\omega\bar{u} < (1+\omega)u_v + \lambda_v$	then	$\bar{z} = u_v$
if	$(1+\omega)u_v + \lambda_v < 2\omega\bar{u} < (1+\omega)u_p + \lambda_v$	then	$\bar{z} = \frac{2\omega\bar{u}-\lambda}{1+\omega}$
if	$(1+\omega)u_p + \lambda_v < 2\omega\bar{u} < (1+\omega)u_p + \lambda_v + \lambda_p$	then	$\bar{z} = u_p$
if	$(1+\omega)u_p + \lambda_v + \lambda_p < 2\omega\bar{u}$	then	$\bar{z} = \frac{2\omega\bar{u}-\lambda_v-\lambda_p}{1+\omega}$.

4 Numerical results

First we consider the influence of the moisture content, M_v, defined as the ratio of the weight of water absorbed to the weight of dry wood in a case without wind and slope. The

numerical calculation corresponds to a square fuel bed of 3×3 m^2 composed with *Pinus Pinaster* with a fuel load of 1 kg/m^2. We have studied the propagation of a fire front for different moisture contents, neglecting first the pyrolysis heat. We used the following set of parameters:

$$K = 0.1JK^{-1}s^{-1},\ \ C = 1300Jkg^{-1},\ \ h = 15Jm^{-2}K^{-1}s^{-1}$$

$$T_\infty = 300K,\ \ T_v = 373K,\ \ T_p = 500K$$

$$M_v = 0.10,\ 0.15,\ 0.20,\ \ \Lambda_v = 2.25 \times 10^6 Jkg^{-1},\ \ \Lambda_p = 0.,\ 3.0 \times 10^4 Jkg^{-1}$$

$$H = 0.2m,\ \ \beta = 0.2s^{-1}\,.$$

We take the time scale $[t] = 1$ s and the length scale $[l] = 1$ m which gives the following non-dimensional parameters:

$$\kappa = 1.3 \times 10^{-4},\ \ \alpha = 0.02,\ \ \lambda_v = 0.6,\ 0.9,\ 1.2,\ \ \lambda_p = 0.,\ 0.09\,.$$

δ represents an empirically set parameter. This parameter takes into account flame and fuel properties, particularly the temperature of the flame T_f and the absorption coefficient a, and it is adjusted for a given fuel in accordance with the rate of spread. The fire is ignited at the center of the square. We obtain a circular fire front as it is foreseen. In *Figure 2* we have plotted the non dimensional temperature on the line $x_2 = x_1$ at different time steps for $M_v = 0.1$. The effect of the moisture content can be clearly appreciated in the plate before the fire front. In *Figure 3* we present the temperature profile at time 150 s for different moisture contents. For the three values of M_v, 0.1, 0.15 and 0.2 considered the rate of spread are 1.07 cm/s, 0.76 cm/s, 0.49 cm/s respectively. For a given fuel load there is an upper value of fuel moisture above which the fire will not propagate; in this example this critical value is $M_v = 0.22$. The heat absorbed by pyrolysis is usually much lower than the heat absorbed by evaporation of water and is sometimes neglected or emulated by an equivalent heat mechanism modifying the specific heat. To see the effect of the pyrolysis heat we show in *Figure 4* for $M_v = 0.05$ and for $\Lambda_p = 0$ and $\Lambda_p = 30$ kJ/kg the position of the fire front at time 150 s. This affects the critical value for the moisture content.

In the second example the influence of the slope and the wind is considered. The slope modifies the nonlocal radiation term in a similar manner as does the wind, so the effect in the propagation of the fire front is similar. The wind has two effects, in one hand through the convective term, on the other hand determine the tilt angle of the flame, increasing or decreasing nonlocal radiation. We take a terrain surface given by $z = x_2 \tan(\varphi)$ representing an inclined table. φ is the inclination angle of the table. The dimension of the table is $3 \times 3\ m^2$. A wind velocity above the table is considered in the x_1 direction. The parameters δ and β are adjusted so that the rate of spread as a function only of the slope angle and only of the wind velocity fit the values given in [9]. We show in *Figure 5* the maximum rate of spread for an slope angle $\varphi = \pi/6$ and several wind velocities. The contours of the temperature are showed in *Figure 6*. This numerical results agrees reasonably with the images of the experiment described in [9].

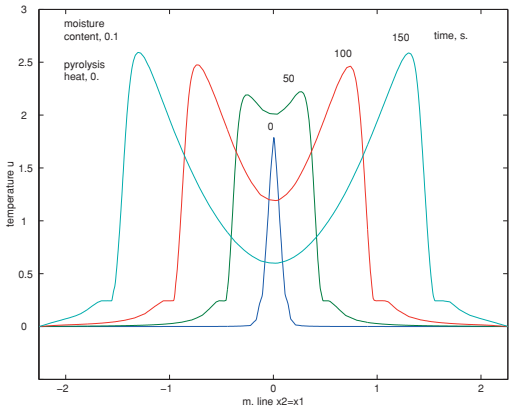

Figure 2: Temperature at different time steps for $M_v = 0.1$

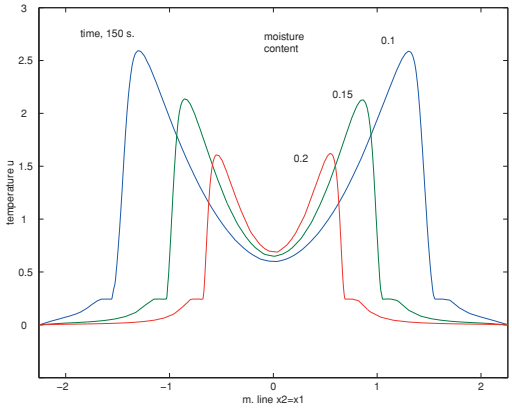

Figure 3: Temperature at time 150 s for different moisture contents

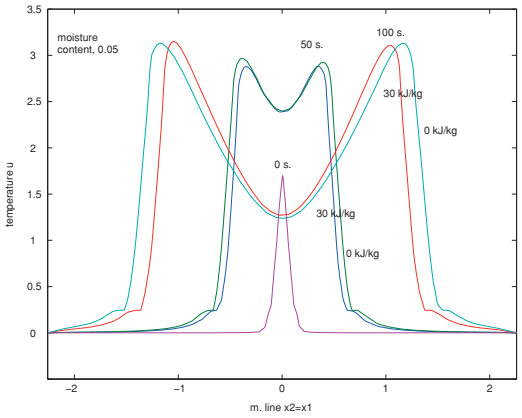

Figure 4: Temperature at times 50 s and 100 s for different pyrolysis heat

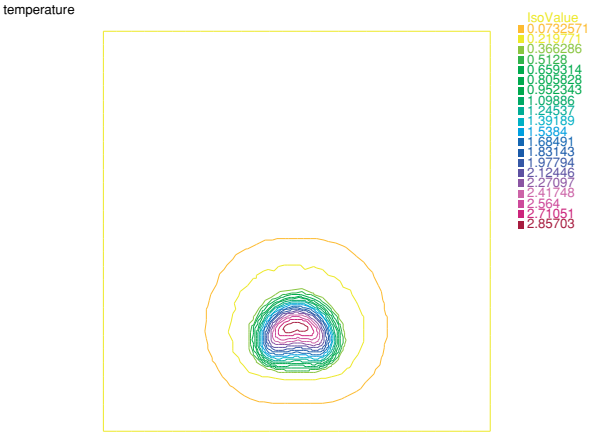

Figure 5: Front position and isotherms at time 50 s

All the computations have been done using P1-Lagrange finite elements approximation, and anisotropic adaptivity, implemented with FreeFem++, a finite element package by Pironneau and Hetcht [13].

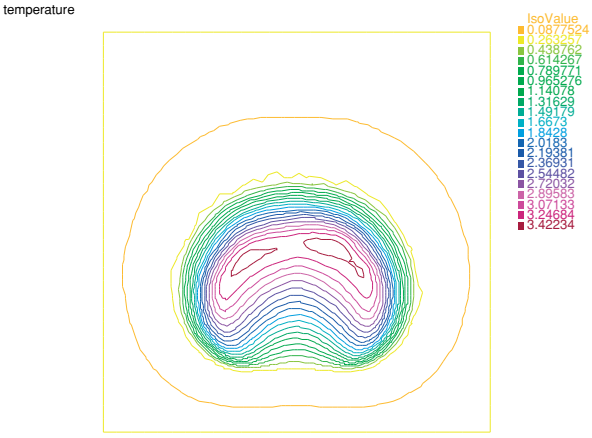

Figure 6: Front position and isotherms at time 100 s

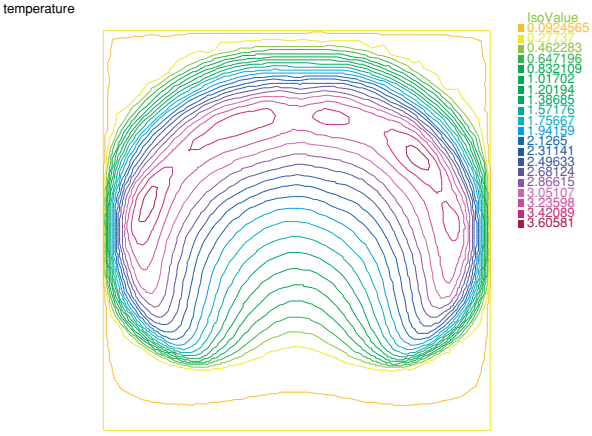

Figure 7: Front position and isotherms at time 150 s

5 Simplified model: enthalpy-radiation model

5.1 Physical model

Let $Q = [0, l_x] \times [0, l_y] \subset R^2$ a rectangle and S be a surface defined by the mapping

$$\begin{aligned} S: \ Q &\longmapsto R^3 \\ x, y &\longmapsto (x, y, h(x, y)) \end{aligned}$$

representing the part of the terrain where the propagation of a fire can take place (see Figure 8). We will assume that vegetation can be represented by a given fuel load M (kg/m^2), together with a moisture content M_v, (kg of water / kg of dry fuel). M and M_v are scalar functions defined on Q. Besides we will assume that the height of the flames in a particular fire is known and bounded by H. In order to take into account some three dimensional effects, and particularly the radiation from the flames above the surface S, we will consider the following three dimensional domain

$$D = \{(x, y, z) \in R^3 \quad (x, y) \in Q, \quad h(x, y) < z < h(x, y) + H\}.$$

In the following sections we develop a model for fire propagation considering the energy and mass conservation equations in the surface S, and the radiation equation in D. We denote, as usual, the boundaries by the symbol ∂.

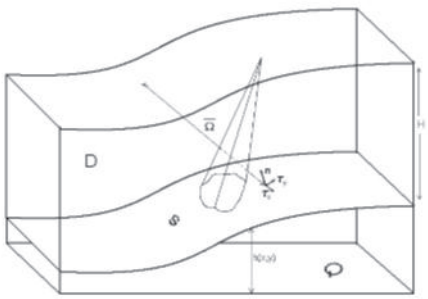

Figure 8: Fire domain

5.2 Energy equations

As the front of pyrolysis and the front of drying are assumed to be sharp we have neglected heat conduction in the vegetation. Energy conservation is described by the equations:

$$\partial_t e + \alpha u = r \quad \text{in } S, \quad t \in (0, t_{max}) \tag{5.1}$$

$$e \in G(u) \quad \text{in } S, \quad t \in (0, t_{max}). \tag{5.2}$$

The initial condition is given by the Arrhenius law:

$$u(\mathbf{x}, 0) = u_0(\mathbf{x}) \quad \mathbf{x} \in S\,. \tag{5.3}$$

The unknowns $e = \frac{E}{MCT_\infty}$ and $u = \frac{T - T_\infty}{T_\infty}$ are the non-dimensional enthalpy and the non-dimensional temperature.

The non-dimensional enthalpy e is an element of a multivalued maximal monotone operator G, given by:

$$G(u) = \begin{cases} u & \text{if} \quad u < u_v \\ [u_v\ ,\ u_v + \lambda_v] & \text{if} \quad u = u_v \\ u + \lambda_v & \text{if} \quad u_v < u < u_p \\ [u_p + \lambda_v\ ,\ u_p + \lambda_v + \lambda_p] & \text{if} \quad u = u_p \\ u + \lambda_v + \lambda_p & \text{if} \quad u > u_p\,. \end{cases}$$

Where u_v and u_p, are the non-dimensional evaporation temperature of the water and the non-dimensional pyrolysis temperature of the solid fuel, respectively. The quantities λ_v and λ_p are the non-dimensional evaporation heat and pyrolysis heat, respectively and are related to the physical quantities by

$$\lambda_v = \frac{M_v \Lambda_v}{CT_\infty}$$

$$\lambda_p = \frac{\Lambda_p}{CT_\infty}$$

It should be noticed that in the burnt zone the multivalued operator does not exactly represent the physical phenomena as the water vapor is no more in the porous medium. This drawback can be circumvented setting $\lambda_v = 0$ and $\lambda_p = 0$ in the burnt area.
The term αu represents the energy lost by convection in the vertical direction. The parameter α is related to physical quantities by $\alpha = \frac{h[t]}{MC}$.

5.3 *Fuel equation*

The mass fraction of solid fuel y, is given by

$$\partial_t y = -g(u)y \qquad \text{in } S \quad t \in (0, t_{max}) \tag{5.4}$$

$$y(x, 0) = y_0(\mathbf{x}) \qquad \mathbf{x} \in S\,. \tag{5.5}$$

Equation (5.4) represents the fuel mass variation due to pyrolysis and (5.5) is the corresponding initial condition. g is given by the Arrhenius law $g(u) = (u > u_p)(y > y_e)\beta exp(-\gamma/(1+u))$ where y_e is the mass fraction lower bound of extinction and the logic expressions are equal to 1 if the expression is true and 0 if the expression is false. γ is related to the activation energy E_a, by $\gamma = \frac{E_a}{RT_\infty}$, R being the universal constant of perfect gases.

5.4 *Radiation*

The right hand side of equation (5.1) describes the thermal radiation reaching the surface S from the flame above the layer. The intensity is defined as the radiadion energy passing through an area per unit time, per unit of projected area and per unit of solid angle. The projected area is formed by taking the area that the energy is passing through and projecting it normal to the direction of travel. The unit elemental solid angle is centered about the direction of travel and has its origin at the area element.

After adimensionalization, the radiation equations in the direction Ω can be written as

$$\mathbf{\Omega}.\nabla i + a^* i = \delta(1+u_g)^4 \quad \text{in } D \tag{5.6}$$

$$i = 0 \quad \text{on } \partial D \cap \{\mathbf{x};\ \mathbf{\Omega}.\mathbf{n} < 0\} \tag{5.7}$$

where $i = \frac{I[t]}{MCT_\infty}$, $a^* = [l]a$ and $\delta = \frac{[l][t]a\sigma[T]^3}{MC\pi}$. $u_g = \frac{T_g - T_\infty}{T_\infty}$ is the non dimensional flame temperature. In a first approximation we have considered a gray body and neglected the scattering. Here, $a(\mathbf{x})$ is the mean absortion coefficient of the gray body and is a function of the point $\mathbf{x} = (x, y, z) \in D$. $\sigma = 5,6699 \times 10^{-8}\ Wm^{-2}K^{-4}$ is the Stefan-Boltzmann constant. The right hand side represents the total emissive power of a blackbody. The incident energy at a point $\mathbf{x}(x, y, h(x, y))$ of the surface S due to radiation from the flame above the surface per unit time and per unit area will be obtained summing up the contribution of all directions $\mathbf{\Omega}$, that is

$$r(\mathbf{x}) = \int_{\omega=0}^{2\pi} i(\mathbf{x}, \mathbf{\Omega})\mathbf{\Omega}.\mathbf{n}\ d\omega\,, \tag{5.8}$$

where we have only considered the hemisphere above the fuel layer.

6 Numerical method

6.1 *Time integration*

Let $\Delta t = t^{n+1} - t^n$ a time step and let y^n, e^n and u^n denote approximations at time step t^n, to the exact solution y, e and u respectively.
We consider a semi-implicit scheme. At each time step we solve,

$$\frac{e^{n+1} - e^n}{\Delta t} + \alpha u^{n+1} = r^n \tag{6.1}$$

$$e^{n+1} \in G(u^{n+1}) \tag{6.2}$$

$$\frac{y^{n+1} - y^n}{\Delta t} = -y^{n+1} g(u^{n+1})\,. \tag{6.3}$$

The basic idea is to treat implicitly the positive terms. The nonlocal radiation term r, depends strongly on the temperature u and on the fuel mass y, therefore, it will be evaluated explicitly at time t^n and its computation is explained in subsection 5.4. Once

the radiation r^n is given, problem (6.1,6.2,6.3) is non linear due to the multivalued operator G. However, the solution of this problem can be reduced to explicit calculations as it is explained in the next subsection.

6.2 *Solution at each time step*

The multivalued operator in (6.2) is maximal monotone, then its resolvent $J_\lambda = (Id+\lambda G)^{-1}$ for any $\lambda > 0$ is a well defined univalued operator. Morever, the Yosida approximation of G, $G_\lambda = \frac{Id-J_\lambda}{\lambda}$ is a Lipschitz operator and the inclusion (6.2) is equivalent for all $\lambda > 0$ to the equation

$$e^{n+1} = G_\lambda(u^{n+1} + \lambda e^{n+1}), \tag{6.4}$$

or

$$u^{n+1} = J_\lambda(u^{n+1} + \lambda e^{n+1}). \tag{6.5}$$

On the other hand, rearranging (6.1) we have

$$u^{n+1} + \frac{1}{\alpha\Delta t}e^{n+1} = \frac{1}{\alpha\Delta t}e^n + \frac{1}{\alpha}r^n. \tag{6.6}$$

Taking $\lambda = 1/(\alpha\Delta t)$ by substitution in (6.5) we obtain

$$u^{n+1} = J_{1/\alpha\Delta t}(\frac{1}{\alpha\Delta t}e^n + \frac{1}{\alpha}r^n). \tag{6.7}$$

Once u^{n+1} has been obtained by solving (6.7) we calculate e^{n+1} and y^{n+1} explicitly

$$e^{n+1} = e^n - \alpha\Delta t u^{n+1} + \Delta t r^n, \tag{6.8}$$

$$y^{n+1} = \frac{y^n}{1 + \Delta t g(u^{n+1})}. \tag{6.9}$$

6.3 *Practical computation of* $J_{1/\alpha\Delta t}(\frac{1}{\alpha\Delta t}e^n + \frac{1}{\alpha}r^n)$

It remains to explain how to calculate u^{n+1} in (6.7). That is, for a given $b = \frac{1}{\alpha\Delta t}e^n + \frac{1}{\alpha}r^n$, compute $s = J_{1/\alpha\Delta t}(b)$, which is equivalent to solve

$$(\alpha\Delta t\ Id + G)s \ni \bar{b} = \alpha\Delta t\ b \tag{6.10}$$

Then s is given by (Figure 9)

$$\begin{array}{lll}
\text{if} \quad \bar{b} < (1+\alpha\Delta t)u_v & \text{then} & s = \frac{\bar{b}}{1+\alpha\Delta t} \\
\text{if} \quad (1+\alpha\Delta t)u_v < \bar{b} < (1+\alpha\Delta t)u_v + \lambda_v & \text{then} & s = u_v \\
\text{if} \quad (1+\alpha\Delta t)u_v + \lambda_v < \bar{b} < (1+\alpha\Delta t)u_p + \lambda_v & \text{then} & s = \frac{\bar{b}-\lambda_v}{1+\alpha\Delta t} \\
\text{if} \quad (1+\alpha\Delta t)u_p + \lambda_v < \bar{b} < (1+\alpha\Delta t)u_p + \lambda_v + \lambda_p & \text{then} & s = u_p \\
\text{if} \quad (1+\alpha\Delta t)u_p + \lambda_v + \lambda_p < \bar{b} & \text{then} & s = \frac{\bar{b}-\lambda_v-\lambda_p}{1+\alpha\Delta t}\,.
\end{array}$$

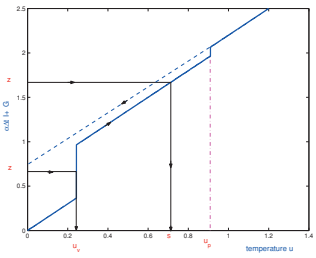

Figure 9: $\alpha\Delta t\ Id + G$ operator

6.4 *Numerical solution of the radiation equation*

The radiation term r in the energy equation (5.1) is computed by numerical integration in (5.8). More precisely, at each point $(x, y, h(x, y))$ on the surface S we consider the tangent plane, its corresponding unit tangent vectors

$$\boldsymbol{\tau}_x = \frac{(1, 0, \frac{\partial h}{\partial x})^t}{\sqrt{1 + (\frac{\partial h}{\partial x})^2}}, \quad \boldsymbol{\tau}_y = \frac{(0, 1, \frac{\partial h}{\partial y})^t}{\sqrt{1 + (\frac{\partial h}{\partial y})^2}},$$

and the unit normal

$$\mathbf{n} = \frac{(-\frac{\partial h}{\partial x}, -\frac{\partial h}{\partial y}, 1)^t}{\sqrt{1 + (\frac{\partial h}{\partial x})^2 + (\frac{\partial h}{\partial y})^2}}.$$

In the corresponding axes the directions $\boldsymbol{\Omega}$ can be expressed

$$\boldsymbol{\Omega} = c_1\boldsymbol{\tau}_x + c_2\boldsymbol{\tau}_y + c_3\mathbf{n}, \quad c_3 \geq 0,$$

where $c_1,\ c_2,\ c_3$ are determined by the couple (θ, ϕ) with $0 \leq \theta \leq \pi/2$ being the angle of $\boldsymbol{\Omega}$ with $\mathbf{n}$ (polar angle) and $0 \leq \phi \leq 2\pi$ the angle of the projection of $\boldsymbol{\Omega}$ on the tangent plane (azimuthal angle), with $\boldsymbol{\tau}_x$ (10).

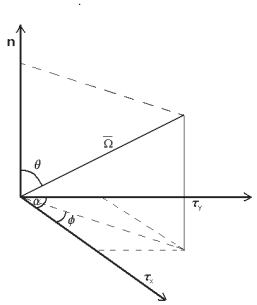

Figure 10: tangent space

To be more specific, let us denote $\mu = \cos\theta$, $\gamma = \cos\phi$, and $\varsigma = \cos\alpha = \boldsymbol{\tau}_x \cdot \boldsymbol{\tau}_y$, that is, α is the angle between the two tangent vectors. Then the expression of $\boldsymbol{\Omega}$ in the base $\{\boldsymbol{\tau}_x, \boldsymbol{\tau}_y, \mathbf{n}\}$ is

$$\boldsymbol{\Omega} = (1-\mu^2)^{1/2}\frac{\gamma\sqrt{1-\varsigma^2} - \varsigma\sqrt{1-\gamma^2}}{\sqrt{1-\varsigma^2}}\boldsymbol{\tau}_x + (1-\mu^2)^{1/2}\frac{\sqrt{1-\gamma^2}}{\sqrt{1-\varsigma^2}}\boldsymbol{\tau}_y + \mu\mathbf{n}, \tag{6.11}$$

which gives the following expression for the cartesian components

$$\boldsymbol{\Omega} = (\Omega_1, \Omega_2, \Omega_3)^t,$$

where

$$\Omega_1 = \frac{-\mu}{\sqrt{1+(\frac{\partial h}{\partial x})^2+(\frac{\partial h}{\partial y})^2}}\frac{\partial h}{\partial x} + \frac{1}{\sqrt{1+(\frac{\partial h}{\partial x})^2}}\frac{\gamma\sqrt{1-\varsigma^2} - \varsigma\sqrt{1-\gamma^2}}{\sqrt{1-\varsigma^2}},$$

$$\Omega_2 = \frac{-\mu}{\sqrt{1+(\frac{\partial h}{\partial x})^2+(\frac{\partial h}{\partial y})^2}}\frac{\partial h}{\partial y} + \frac{1}{\sqrt{1+(\frac{\partial h}{\partial y})^2}}\frac{\sqrt{1-\mu^2}\sqrt{1-\gamma^2}}{\sqrt{1-\varsigma^2}},$$

$$\Omega_3 = \frac{\mu}{\sqrt{1+(\frac{\partial h}{\partial x})^2+(\frac{\partial h}{\partial y})^2}} + \frac{\sqrt{1-\mu^2}}{\sqrt{1+(\frac{\partial h}{\partial x})^2}}\frac{\gamma\sqrt{1-\varsigma^2} - \varsigma\sqrt{1-\gamma^2}}{\sqrt{1-\varsigma^2}}\frac{\partial h}{\partial x} + \ldots$$

$$\ldots + \frac{1}{\sqrt{1+(\frac{\partial h}{\partial y})^2}}\frac{\sqrt{1-\mu^2}\sqrt{1-\gamma^2}}{\sqrt{1-\varsigma^2}}\frac{\partial h}{\partial y}.$$

Finally, summing up for all the solid angles in (5.8)

$$r(\bar{\mathbf{x}}) = \int_{\theta=0}^{\theta=\pi/2}\int_{\phi=0}^{\phi=2\pi} i(\bar{\mathbf{x}},\theta,\phi)\cos\theta\sin\theta\; d\theta d\phi =$$

$$\int_{\mu=0}^{\mu=1}\int_{\gamma=-1}^{\gamma=1}\frac{i_+(\bar{\mathbf{x}},\mu,\gamma)\mu}{\sqrt{1-\gamma^2}}\,d\mu d\gamma \;+\; \int_{\mu=0}^{\mu=1}\int_{\gamma=-1}^{\gamma=1}\frac{i_-(\bar{\mathbf{x}},\mu,\gamma)\mu}{\sqrt{1-\gamma^2}}\,d\mu d\gamma \tag{6.12}$$

where i_+ (resp. i_-) stands for the radiation intensity i corresponding to an angle ϕ such that $0 \leq \phi < \pi$ (resp. $\pi \leq \phi < 2\pi$). The integrals in (6.12) are computed using Gauss-Legendre quadrature with respect to μ and Gauss-Chebyshev quadrature with respect to γ in order to cope with the singular weight $\frac{1}{\sqrt{1-\gamma^2}}$. That is

$$r(\bar{\mathbf{x}}) \approx \sum_{k,l} W_{kl}\, i_+(\bar{\mathbf{x}}, \mu_k, \gamma_l)\mu_k + \sum_{k,l} W_{kl}\, i_-(\bar{\mathbf{x}}, \mu_k, \gamma_l)\mu_k. \tag{6.13}$$

Characteristics method

To compute the incident radiation in the direction $\mathbf{\Omega}$ at a point on the surface S $(\bar{x}, \bar{y}, \bar{z})$, with $\bar{z} = h(\bar{x}, \bar{y})$, we consider the characteristic line

$$[0, \xi] \longmapsto \mathcal{R}^3$$

$$\xi \longrightarrow (x(\xi) = \bar{x} + \xi\Omega_1,\ y(\xi) = \bar{y} + \xi\Omega_2,\ z(\xi) = \bar{z} + \xi\Omega_3)\,.$$

On the characteristic, equation (5.6) becomes

$$\frac{di}{d\xi} + a^* i = \delta(1 + u_g)^4, \tag{6.14}$$

which can be solved together with the condition

$$\lim_{\tau \to \infty} i(\xi) = 0. \tag{6.15}$$

To solve the problem, we need to evaluate the gas temperature u_g in the domain D. The solution of the energy and fuel equations (5.1, 5.2, 5.4) only provides the temperature u on the surface S. To extend the temperature field to the whole domain D we proceed as follows: If there is no wind, we extend the temperature vertically, that is, we define the extension $\tilde{u}$ by $\tilde{u}(x, y, z) = u(x, y, h(x, y))$ for all points $(x, y, z) \in D$ and $h(x, y) < z < h(x, y) + H$. In the case of wind conditions, we compute the extended field assuming a convective transport, that is, $\tilde{u}(x, y, z) = u(x - (z - h(x, y))\frac{v_x}{v_z}, y - (z - h(x, y))\frac{v_y}{v_z}, h(x, y))$. Here (v_x, v_y, v_z) stands for the velocity field which we suppose to be known. More precisely, (v_x, v_y) is a horizontal meteorological velocity field and v_z is computed by the rule $v_z \sim \sqrt{10H}$. Otherwise a three-dimensional velocity field can be computed involving only two-dimensional computations using for example the model in [14].

6.5 Example 1: Fire propagation in the Ebro River Basin

In this example we consider the fire propagation in a zone of the Ebro river basin where the combined effects of the topography, wind and radiation can be observed. First due to the wind the fire front follows the river bed. Later the wind turns and by effect of radiation the fire crosses the river and rises up to the top of the mountain.

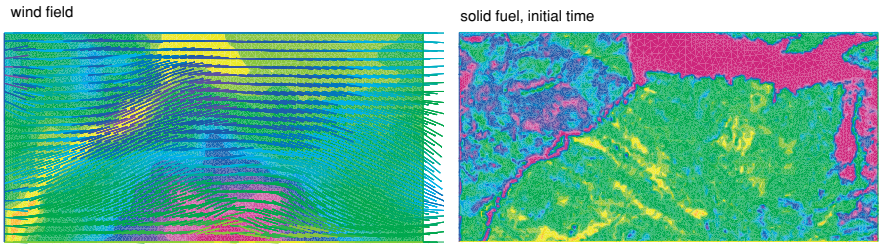

Figure 11: Wind field, topography and initial fuel distribution

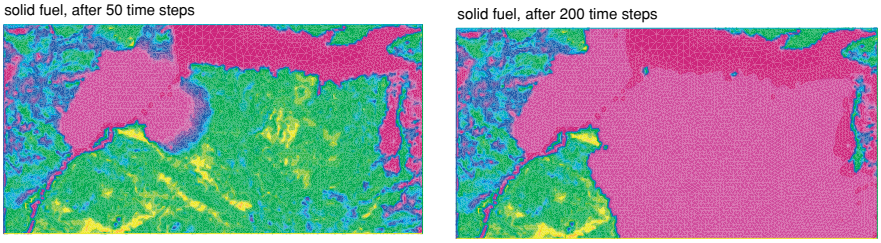

Figure 12: Fuel distribution and burned zone after 50 and 200 time steps

6.6 Example 2: Parallel computing perfomance of the radiation term

In this example we consider the parallel computation of the radiation term and its efficiency. The example corresponds to a fire near the village of Cofrentes in the center of Spain. Main physical parameters are:

- Zone 6 km long by 3 km width
- Water content: 2%
- Half-time decay: 700 seconds
- Flame height: 20 meters
- Flame temperature 1225^{o}C
- Wind velocity (1st): NO WIND
- Wind velocity (2nd): 10 m/s $\div$ 20 m/s

Main numerical data are:

- Mesh size: maximum size 100 meters, minimum size 50 meters
- number of uknowns per variable: 31774
- Time step: 200 seconds
- Numerical integration points for radiation: $8 \times 2 = 16$.

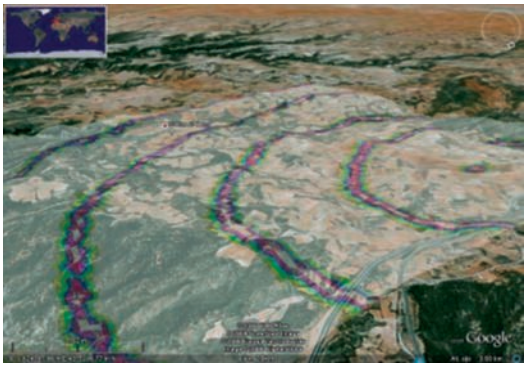

Figure 13: Fire front position without wind

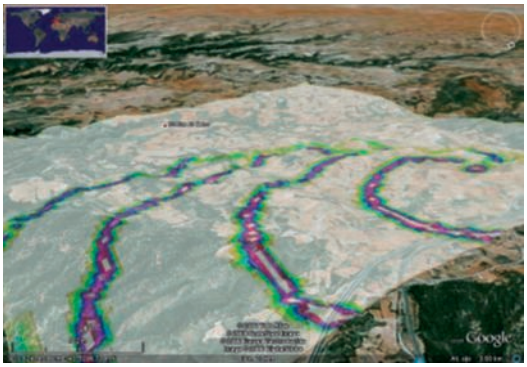

Figure 14: Fire front position with wind

Number of threads	Run Time (seconds)	Acceleration	Efficiency
1	3.798	1	100%
4	1.110	3,42	86%
8	681	5,57	70%
16	687	5,53	35%

Table 1: Run times and efficienty for eight directions of numerical integration

Number of threads	Run Time (seconds)	Acceleration	Efficiency
1	12.265	1	100%
4	3.220	3,81	95%
8	1.770	6,93	87%
16	1.606	7,64	48%

Table 2: Run times and efficiency for sixteen directions of numerical integration

Appendix

In this appendix we estimate the nonlocal radiation term R in equation (5.1). In a non scattering medium, for a gray gas, the incident radiation intensity at a given point of the terrain surface for a fixed direction, integrated over all wavelengths, is given by (see[12], and *Figure 7*):

$$i(\mu) = i(0)e^{-\mu} + \int_0^{\mu} i_b(\mu^*)e^{-(\mu-\mu^*)}d\mu^*\,, \tag{6.16}$$

where a is the absorption coefficient, $\mu(s) = \int_0^s a(s^*)ds^*$ is the optical thickness for a path of length s, and i_b is the intensity radiation from a black body.
Assuming that the gas out of the flame is a transparent medium, then $i(0) = 0$ and taking into account that inside the flame $i_b(\mu) = \frac{\sigma T_{fl}^4(\mu)}{\pi}$ we obtain assuming a flame with small width

$$i(\mu(s)) = \frac{\sigma T_{fl}^4}{\pi}(1 - e^{-a(s_2-s_1)}) \approx \frac{a\sigma T_{fl}^4}{\pi}(s_2 - s_1)\,,$$

where $s_2 - s_1$ is the travel length inside the flame.
The energy flux q at a point $\mathbf{P}(\mathbf{x}, z)$ of the terrain surface is obtained integrating for all directions

$$q = \int_{\theta=0}^{\theta=2\pi}\int_{\beta=\beta_H}^{\beta=\pi/2} i(\beta,\theta)\cos(\beta)\sin(\beta)d\beta d\theta\,.$$

For a flame with triangular section of vertex $\mathbf{V}$ and base centered in $\mathbf{O}$, see *Figure 8*, setting α_f the angle between the flame and the horizontal plane, γ the angle between the horizontal projection of the flame with the position vector of the point $\mathbf{x}$ with respect to

the center of the base of the flame, α_s the slope of the terrain surface, and B the width of the flame base, we get

$$q(\mathbf{x}) = \frac{a\sigma T_f^4}{\pi} \int_0^{2\pi} \int_{\beta_H}^{\pi/2} \frac{B \sin\beta(\tan\beta - \tan\beta_H)}{(\frac{\cos\gamma + \tan\alpha_f \tan\alpha_s}{\tan\alpha_f - \cos\gamma \tan\alpha_s} + \tan\beta)^2 - (\frac{B}{2H})^2} d\beta d\theta \,. \tag{6.17}$$

Now using a Simpson rule to integrate with respect to β and observing that $d\theta = \dfrac{d\tilde{A}}{B\|\mathbf{x} - \tilde{\mathbf{x}}\|}$ we obtain

$$q(\mathbf{x}) = \frac{a\sigma T_f^4}{\pi} \int_{\Omega_f} \frac{g(\alpha, \gamma, \alpha_s, \beta_H)}{\|\mathbf{x} - \tilde{\mathbf{x}}\|} d\tilde{A} \,, \tag{6.18}$$

where

$$g(\alpha_f, \gamma, \alpha_s, \beta_H) = \frac{2}{3}(\frac{\pi}{2} - \beta_H) \frac{\sin(\frac{\beta_H + \frac{\pi}{2}}{2})(\tan(\frac{\beta_H + \frac{\pi}{2}}{2}) - \tan\beta_H)}{(\frac{\cos\gamma + \tan\alpha_f \tan\alpha_s}{\tan\alpha_f - \cos\gamma \tan\alpha_s} + \tan(\frac{\beta_H + \frac{\pi}{2}}{2}))^2}$$

and $\beta_H = \arg\tan(\frac{\|x - \tilde{x}\|}{H} - \frac{\cos\gamma + \tan\alpha_f \tan\alpha_s}{\tan\alpha_f - \cos\gamma \tan\alpha_s})$.
Finally the expression for R in (5.1) is obtained by adimensionalization, taking $\delta = \frac{a\sigma T_f^4}{\pi DCT_\infty}[t][l]$ and $f(\mathbf{x} - \tilde{\mathbf{x}}) = \frac{g(\alpha_f, \gamma, \alpha_s, \beta_H)}{\|\mathbf{x} - \tilde{\mathbf{x}}\|}$.

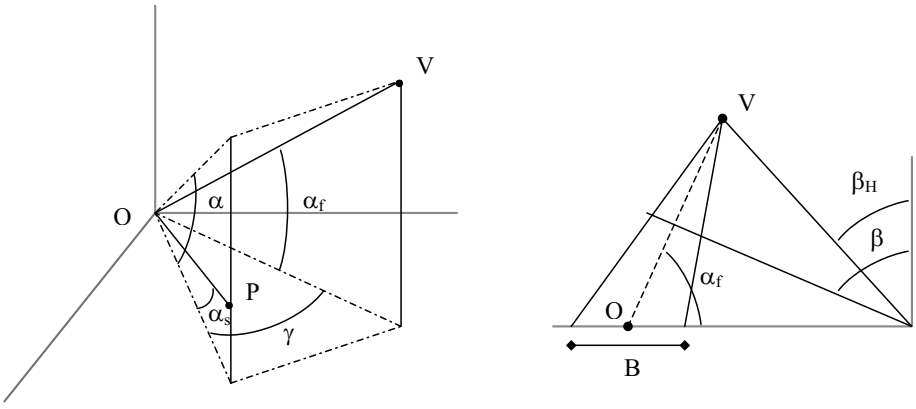

Figure 15: Flame position

REFERENCES

[1] L. Ferragut, M.I. Asensio, S. Monedero, Modelling radiation and moisture content in fire spread. *Commun. Numer. Meth. Eng.*, **23** (2007), 819–833.

[2] L. Ferragut, M.I. Asensio and S. Monedero., *Numerical Methods for the Computation of Radiation and Moisture Effects in Fire Spread*. ECT 2006 V International Conference on Engineering Technology, Las Palmas de Gran Canaria, 12-15 Sept. 2006. Proceedings of The Fifth International Conference on Engineering Computational Technology Edited by B.H.V. Topping, G. Montero and R. Montenegro. Civil-Comp Press, Stirlingshire, United Kingdom, paper 200, 2006

[3] R. R. Linn, *Transport model for Prediction of Wildland Behaviour*. Los Alamos National Laboratory, Scientific Report, LA1334-T, 1997.

[4] J.L. Dupuy, M. Larini. Fire spread through a porous forest fuel bed: a radiation and convective model including fire-induced flow effects. *Int. J. of Wildland Fire*, 1999, **9**: 155-172.

[5] J.H. Balbi, F. Morandini, P.A. Santoni, A. Simenoni. Two dimensional fire spread model including long-range radiation and simplied flow. In *Int. Forest Fire Research and Wildland Fire Safety, Luso, Coimbra*, Viegas (eds). Millpress: Rotterdam, 2002.

[6] J. Margerit, O. Séro Guillaume. Modelling forest fires. Part II: reduction to two-dimensional models and simulation of propagation, *Int. J. Heat and Mass Transfer* 2002; **45**: 1723-1737.

[7] G. Cox. *Combustion Fundamentals of Fire*. Academic Press, London, 1995.

[8] A. Simeoni, M. Larini, P.A. Santoni, J.H. Balbi. Coupling of a simplified flow with a phenomenological fire spread model. *C.R. Mecanique*, 2002, **330**: 783-790.

[9] D.X. Viegas, L.P. Pita, L. Matos, P. Palheiro. Slope and wind effects on fire spread. In *Int. Forest Fire Research and Wildland Fire Safety, Luso, Coimbra* Viegas (eds). Millpress: Rotterdam, 2002.

[10] O. Pironneau. On the Transport-Difussion Algorithm and its applications to the Navier-Stokes Equations. *Numer. Math.*, 1982, **38**: 309-332.

[11] A. Bermúdez, C. Moreno. Duality methods for solving variational inequalities. *Comp. and Math. Appl.* 1981, **7**: 43-58.

[12] R. Siegel, J.R. Howell. *Thermal Radiation Heat Transfer*. McGraw-Hill, New York, 1971.

[13] http://www.freefem.org [10 april 2003].

[14] M.I. Asensio, L. Ferragut, J. Simon, *A convection model for fire spread simulation*, Applied Mathematics Letters, **18** (2005), 673-677.